A Novel Spatial Images Technique for the Analysis of Cavity Backed Antennas

A. Alvarez Melcón and Juan R. Mosig
Laboratoire d'Electromagnétisme et d'Acoustique (LEMA). EPFL, Lausanne, Switzerland

***Abstract*—This paper describes a new contribution to the analysis of arbitrary shielded circuits and antennas of complex shapes, in the frame of the integral equation (IE) and Method of Moments formulation (MoM). The technique is based on the spatial image approach and a new specially truncated set of images is developed to enhance the convergence behavior of the series involved. Results show that, with the new specially truncated series of images, convergence is achieved very fast. In this paper simulated results obtained with the new approach are compared with measurements.**

***Index terms*—Microwave circuits and antennas, shielding, Green function, spatial images, integral equation, method of moments.**

I. Introduction

The analysis of shielded microwave circuits and antennas is a subject that has always attracted much attention and several numerical models have been developed in the past. Among them, finite element techniques have been successfully used [1] but they usually lead to computer codes which are computationally heavy. Perhaps the most popular and efficient technique is the integral equation (IE) formulation combined with the Method of Moments (MoM) algorithm [2]. The main practical difficulty in this approach, however, is in the numerical evaluation of the associated Green's functions usually formulated as very slowly convergent modal series. For the efficient summation of these series the Fast Fourier Transform (FFT) has been successfully used in the past [2],[3], but it restricts the subsequent discretization of the circuits to uniform meshes. Other acceleration techniques, without the use of the FFT, have been recently reported, namely the use of the residue theorem [4] and the use of the Sommerfeld identity [5]. An alternative technique to the modal series approach is to formulate the Green's functions in the spatial domain using the image theory. In this context we can mention the work in [6] who used the Ewalt transformation to sum the spatial images series, but no dielectric layers are considered, and the work in [7] who formulated the spatial images series only to the quasi-static part of the kernel.

In the frame of IE-MoM, we provide in this paper a new contribution to the analysis of arbitrary shielded circuits and antennas of complex shapes. The technique is based on the spatial images approach and it formulates the complete Green's functions associated to a general multilayered medium as standard Sommerfeld integrals. Once Sommerfeld type Green's functions are computed, the effect of lateral walls is locally included by adding spatial images. Care is exercised to ascertain the convergence behavior of the resulting spatial images series. For those cases exhibiting slow convergence behavior, a specially truncated series of images is developed based on the imposition of the boundary conditions for the fields and potentials at specific points on the metallic walls. Results reveal that convergence with the specially truncated set of images is very fast and accurate results are obtained with only 10 spatial images. An interesting feature of the technique developed is that triangular-cell based MoM formulations can be easily used, thus allowing the analysis of arbitrary complex structures. In addition, with the proposed approach all the know-how in the field of Sommerfeld integrals evaluation can be directly put to work for the analysis of shielded structures.

II. Image theory

The key step in the analysis of planar multilayered printed circuits following the space IE approach, is the derivation of the spatial domain Green's functions formulated, in the case of a medium of infinite lateral transverse dimensions, as Sommerfeld integrals [8]. With ref-

A. Alvarez Melcón, 41-21-693-4637, fax 41-21-693-2673, Alejandro.Alvarez-Melcon@epfl.ch. Juan R. Mosig, 41-21-693-4628, fax 41-21-693-2673, Juan.Mosig@epfl.ch. web site: http://lemawww.epfl.ch.

This work was supported by ESA/ESTEC under Contract No. 11698/95/NL/SB, and it was developed in collaboration with the companies ALCATEL ESPACE, France and CASA, Spain.

erence to the shielded structure in Fig. 1, the corresponding Green's functions accounting for the presence of the lateral walls can be written using standard spatial image theory. The Green's functions are therefore again formu-

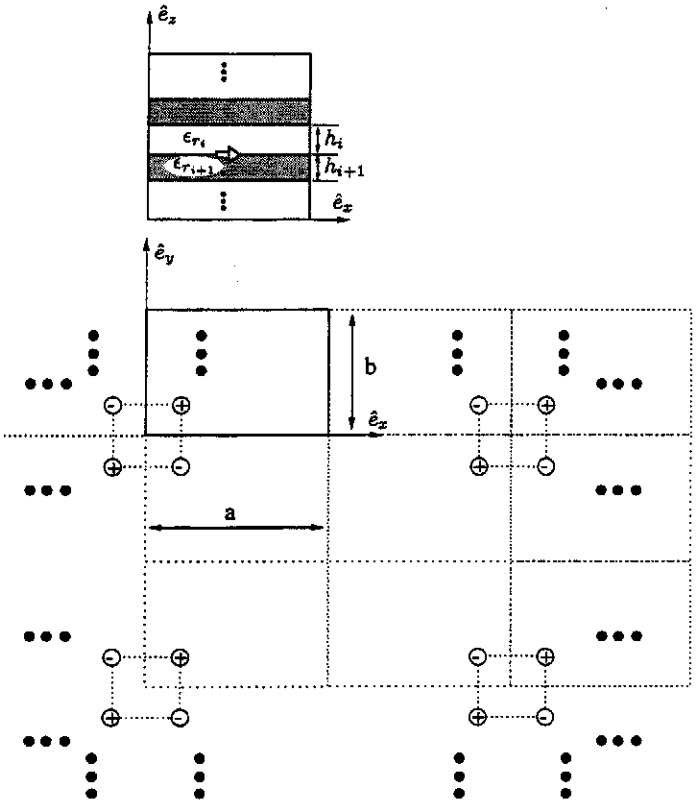

Fig. 1. Basic shielded multilayered structure analyzed in this paper and the associated spatial images for a unit point charge.

lated as Sommerfeld integrals, but they are computed for an extended range of source-observer distances to account for the interaction of all required spatial images. For this purpose asymptotic techniques specially efficient for large source-observer distances are best utilized as described in [9]. The boxed mixed potential Green's functions G_{Box} are then written as [8]

$$\begin{aligned} G_{\text{Box}}(x,y|x',y') = \\ \sum_{m=-\infty}^{\infty}\sum_{n=-\infty}^{\infty}\Big[& G(x,y|+x'+2ma,+y'+2nb) \\ & +s_x\, G(x,y|-x'+2ma,+y'+2nb) \\ & +s_y\, G(x,y|+x'+2ma,-y'+2nb) \\ & +s_x\, s_y\, G(x,y|-x'+2ma,-y'+2nb)\Big], \end{aligned} \tag{1}$$

where G is the corresponding Sommerfeld type Green's function and s_x, s_y are sign functions taking the values shown in Table I for the different types of mixed potential Green's functions components. As shown in (1) the total Green's functions are now expressed in terms of infinite series and the convergence behavior becomes therefore an issue. For instance, we have found convergence problems in the analysis of the microstrip line shown in Fig. 2, printed on a thick dielectric substrate ($\epsilon_r = 3.0$, $h/\lambda = 0.2$).

To illustrate this point, we present in Fig. 3(a) and 3(b) the computed S-parameters when, respectively, 22 and 102 spatial images are included in the analysis. As it can be observed, the ripple in the computed response indicates that convergence rapidly deteriorates with frequency. Moreover, the use of more images does not solve the problem and, as shown in Fig. 3(b), only the ripple is more compressed. This slowly convergence behavior can be explained as being due to the excitation of surface waves in the structure. To easily understand this fact we have computed the associated Green's functions using the imaginary axis decomposition reported in [9]. Following this technique, the total Green's functions are expressed as the sum of three main contributions, namely the quasi-static part, the spatial wave part and the contribution due to the surface waves excitation. Fig. 4 shows the computed electric scalar potential Green's function for two different frequencies. The first one (2 GHz) corresponds to a frequency where convergence is still good while the second one (10 GHz) corresponds to a frequency well inside the ripple region. We can clearly observe that at 2 GHz the surface wave is very weakly excited and it starts to dominate the global Green's function behavior for spatial distances (ρ) of order of ($k_0\,\rho = 100$). Moreover, for small source-observer distances the Green's function exhibit a strong decaying behavior of ($1/\rho^2$) type. On the contrary, at 10 GHz the surface wave is very strongly excited since it dominates the global Green's function behavior for spatial distances of about only ($k_0\,\rho = 1$). In addition, for small source-observer distances the decaying behavior is now inverse of the distance ($1/\rho$), instead of ($1/\rho^2$) as before. Consequently, we can conclude that the convergence properties of the spatial images series are related to the amount of electromagnetic energy coupled to the surface wave modes. To try to overcome this problem, a specially truncated set of images has been developed and it is described in the next section.

TABLE I

Value of the sign functions for all different mixed potential Green's functions components. G_{BA} denotes boxed magnetic vector potential Green's function while G_{BV} is the boxed electric scalar potential.

–	s_x	s_y
G_{BA}^{xx}	+1	−1
G_{BA}^{yy}	−1	+1
G_{BV}	−1	−1

III. Specially Truncated Set of Images

The problem of the slow convergence behavior of the series developed in the previous section can be overcome by noticing that there are two main features in any boxed Green's function that must be preserved in order to obtain accurate results, namely:

1. The singular behavior when $\rho \to 0$.
2. The boundary conditions at all lateral cavity walls.

The singular behavior is naturally preserved in the developed series of images, because they have been constructed using standard Green's functions. What remains then, is the accurate imposition of the boundary conditions at the metallic walls. This can be done by simply adding the first few images of the series as before, and then computing the needed strength of the last remaining images so that the boundary conditions for the fields are strictly satisfied at the projections of the observer points at the metallic walls. To simplify the analytical exposition of the problem we now show the procedure for the case of the electric scalar potential inside a parallel plate waveguide, being formally analogous for the rectangular cavity case. From (1) and Table I we write the electric scalar potential Green's function in the parallel plate waveguide structure shown in Fig. 5, as

$$G_{BV}(x,y|x',y') = \sum_{m=-\infty}^{\infty} \Big[G_V(x,y|+x'+2ma,y') - G_V(x,y|-x'+2ma,y') \Big], \quad (2)$$

where G_V is the Sommerfeld type electric scalar potential Green's function in the layered structure considered. In

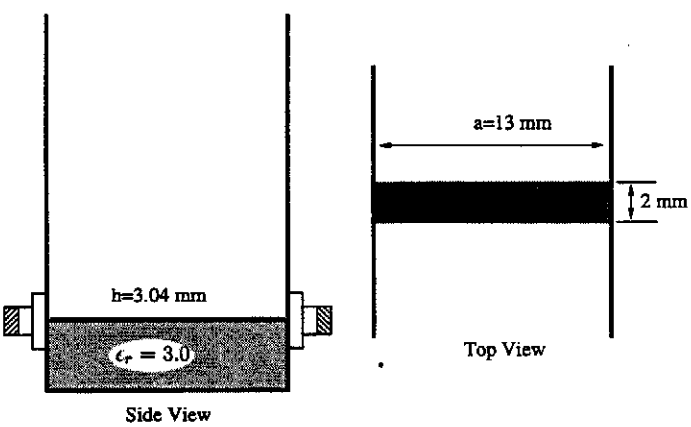

Fig. 2. Microstrip line printed on a thick substrate and backed by a parallel plate waveguide.

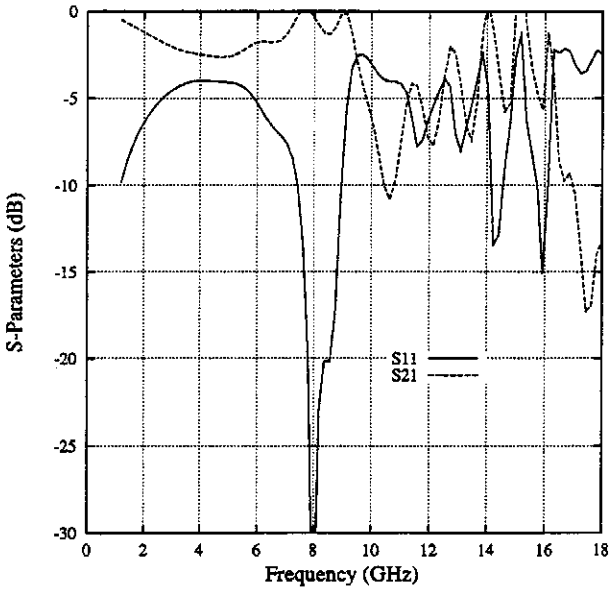

(a) Results with 22 spatial images.

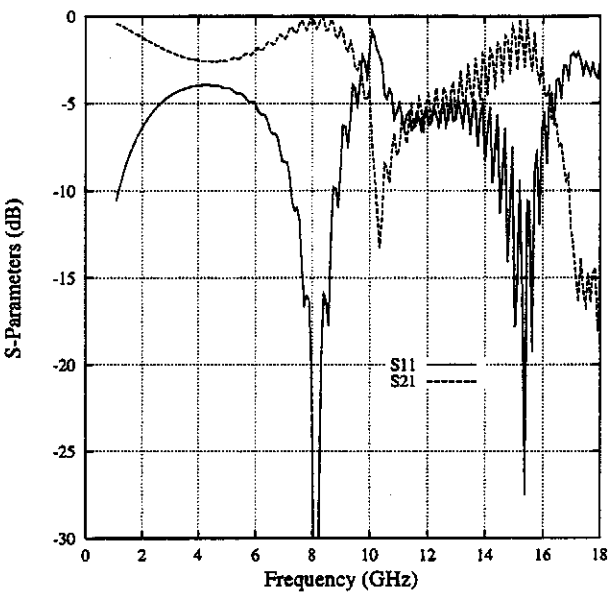

(b) Results with 102 spatial images.

Fig. 3. Scattering parameters of the structure in Fig. 2 when 22 and 102 spatial images are included in the analysis

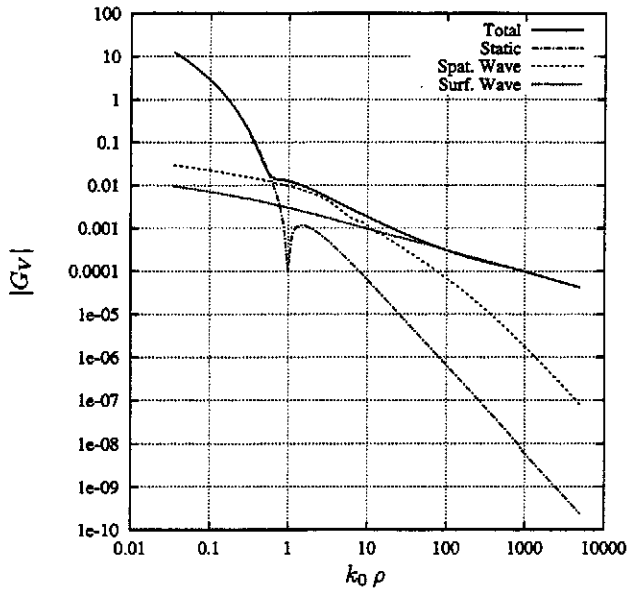

(a) Frequency 2 GHz.

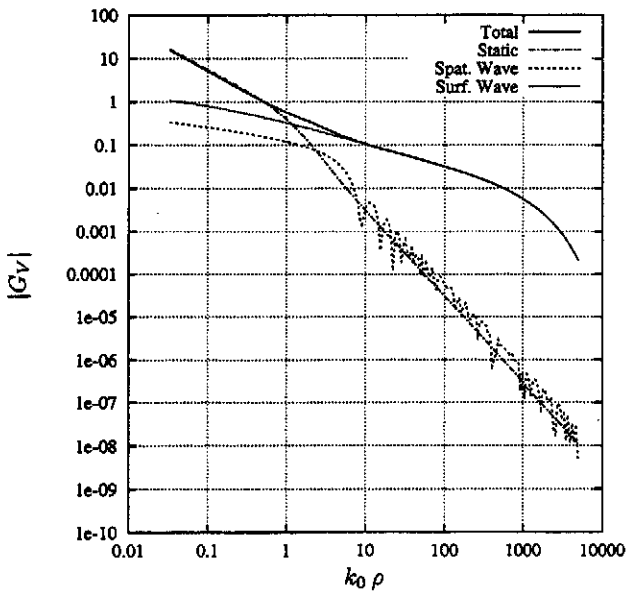

(b) Frequency 10 GHz.

Fig. 4. Imaginary axis decomposition for the electric scalar potential associated to the problem in Fig. 2. Source-observer distance is ρ.

the above equation, it is convenient to define an intermediate Green's function representing the potential created by a basic image couple (basic image set) as (Fig. 5)

$$G_{V_m}^{\text{BIS}}(x,y|x',y') = G_V(x,y|+x'+2ma,y') - G_V(x,y|-x'+2ma,y'), \quad (3)$$

and obviously, this intermediate Green's function matches the boundary conditions at the $x = 0$ wall. To serve our purposes, it is convenient to truncate the infinite spatial series with (M) and rewrite equation (2) using the definition in (3) as

$$G_{\text{BV}}(x,y|x',y') \approx \sum_{m=-M+1}^{+M-1} G_{V_m}^{\text{BIS}}(x,y|x',y') + G_{V_{+M}}^{\text{BIS}}(x,y|x',y') + G_{V_{-M}}^{\text{BIS}}(x,y|x',y'). \quad (4)$$

It is interesting to observe that the spatial images in (4) is balanced with respect the first metallic wall at $(x = 0)$, that is the boundary conditions are already rigorously imposed at this wall. On the contrary, the series is unbalanced with respect the second metallic wall at $(x = a)$. The key idea in this technique is to introduce an unknown constant (q) so that the strength of the two last basic image sets in the series are adjusted to enforce the right boundary condition for the potential also at the second metallic wall. We then introduce the unknown constant (q) and rewrite (4) as

$$G_{\text{BV}}(x,y|x',y') \approx \sum_{m=-M+1}^{+M-1} G_{V_m}^{\text{BIS}}(x,y|x',y') + q\left[G_{V_{+M}}^{\text{BIS}}(x,y|x',y') + G_{V_{-M}}^{\text{BIS}}(x,y|x',y')\right]. \quad (5)$$

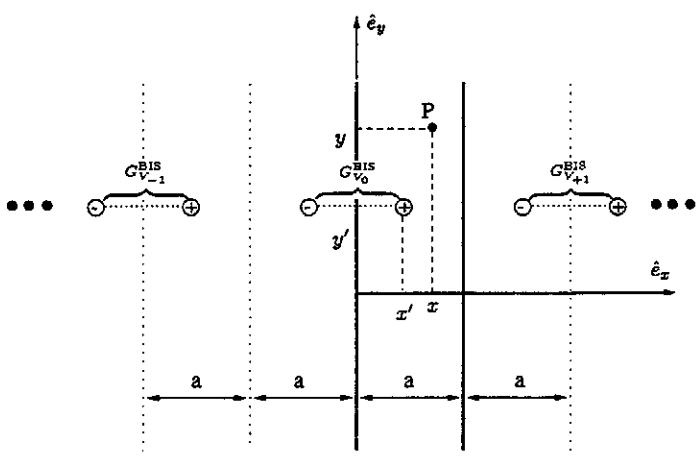

Fig. 5. Spatial images arrangement for a parallel plate waveguide structure.

In (5) the potential created by the first $(2M-1)$ basic image sets can now be defined as

$$\hat{G}_{BV}(x,y|x',y') = \sum_{m=-M+1}^{+M-1} G^{BIS}_{V_m}(x,y|x',y'), \qquad (6)$$

and the potential created by the two last basic image sets as

$$G^{l}_{BV}(x,y|x',y') = q\left[G^{BIS}_{V_{+M}}(x,y|x',y') + G^{BIS}_{V_{-M}}(x,y|x',y')\right]. \qquad (7)$$

Next, the potential created by the first $(2M-1)$ basic image sets at the projection of the observer point at the second metallic wall is computed from (6) as

$$w = \hat{G}_{BV}(a,y|x',y') = \sum_{m=-M+1}^{+M-1} G^{BIS}_{V_m}(a,y|x',y'). \qquad (8)$$

Since the total potential must be zero also at the second metallic wall, the potential created by the two last basic image sets must compensate (8), and thus the following relation can be written

$$-w = q\left[G^{BIS}_{V_{+M}}(a,y|x',y') + G^{BIS}_{V_{-M}}(a,y|x',y')\right], \qquad (9)$$

from where the unknown constant required to annihilate the total potential also at the second metallic wall is easily found as

$$q = \frac{-w}{\gamma_1 + \gamma_2}, \qquad (10)$$

with the redefinitions of the following coefficients

$$\gamma_1 = G^{BIS}_{V_{+M}}(a,y|x',y'), \qquad \gamma_2 = G^{BIS}_{V_{-M}}(a,y|x',y'). \qquad (11)$$

It is important to point out that a similar procedure as the one described here for the electric scalar potential is also applied for those components of the magnetic vector potential satisfying Newman boundary conditions at the metallic walls, and the only difference is that numerical differentiation is used in order to annihilate the total derivative.

To show the effectiveness of the approach developed, we have computed the electric scalar potential Green's function for the structure in Fig. 2 when the direct sum in (4) is used and when the new specially truncated set of images is used. In Fig. 6 we show the results obtained as a function of the observer point position for two different frequencies (10 GHz and 30 GHz), fixed position of the source ($x'/a = 0.107$) and when a total number of 3 and 60 pairs of basic image sets are included in the direct sum, and only 3 pairs of basic image sets in the specially

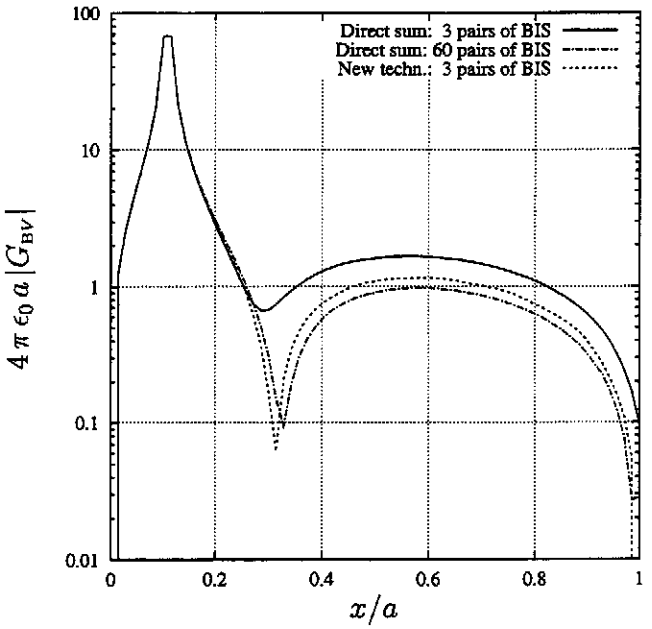

(a) Frequency 10 GHz.

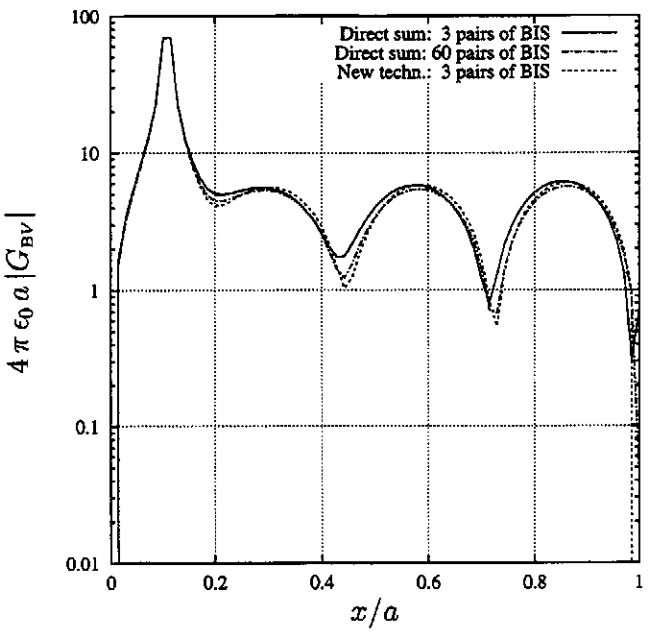

(b) Frequency 30 GHz.

Fig. 6. Shielded electric scalar potential Green's function associated to the problem in Fig. 2 when direct sum is used and when the new specially truncated set of images is used.

truncated series. As we can observe, close to singularity both approaches give similar results, but boundary conditions at the second lateral wall are only satisfied when the specially truncated set of images is used. Also we observe that the oscillations due to the standing wave created by the presence of the lateral walls are slightly readjusted when the specially truncated set of images is used. This readjustment appears to be necessary to allow the potential to be zero at the lateral metallic walls. Finally, it can be observed that when 60 pairs of basic image sets (242 images) are used in the direct sum, the boxed electric scalar potential converges to the results obtained with just 3 specially truncated pairs of basic image sets (14 images), thus indicating the huge saving in computational effort obtained with the new approach.

When the newly developed Green's functions are used in the analysis of the structure in Fig. 2 we observe fast convergence properties in the results. In Fig. 7 we present the computed S-parameters showing very smooth behavior and that the ripple has been effectively canceled out, even with only 3 specially truncated pairs of basic image sets (14 images). By contrast, convergence is not achieved even after 25 pairs of basic image sets (102 images) without truncation as shown in Fig. 3.

To further validate the theory presented, a breadboard of the structure in Fig. 2 has been manufactured and tested. In Fig. 8 we present measured versus simulated results showing good agreement for both S_{11} and S_{21} scattering parameters and with only 3 specially truncated pairs of basic image sets in the calculations.

Finally, it is important to point out that with the proposed approach all additional computations are performed analytically and that the reduction in the number of images required to obtain good convergence is considerable, so that the implementation of efficient software codes is possible.

IV. Results and Discussions

A software code based on the proposed approach has been written for the analysis of complex cavity backed antennas. The asymptotic technique described in [9] has been used for the evaluation of the basic Sommerfeld integrals for large values of source-observer distances and a MoM technique based on triangular cells has been implemented.

To show the usefulness of the technique, we present the analysis of a circular-polarized cavity-backed antenna containing two stacked patches of complex shapes (note in particular the narrow slits existing in both patches). In

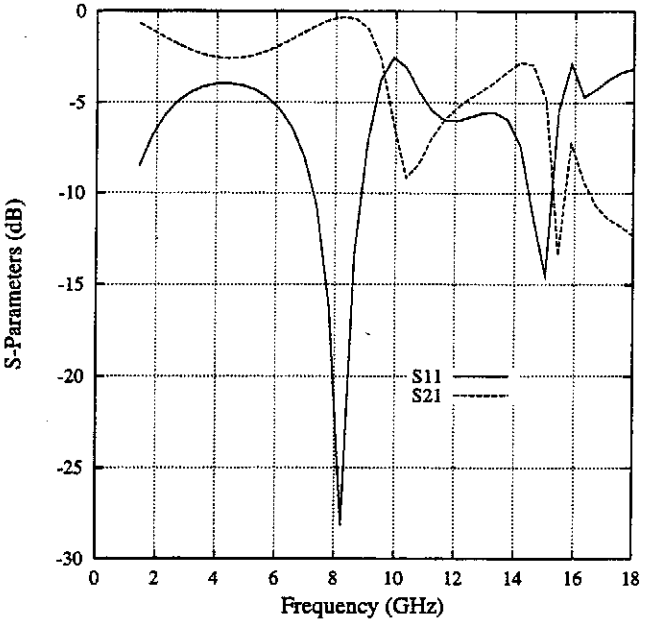

(a) Results with 2 truncated pairs of basic image sets.

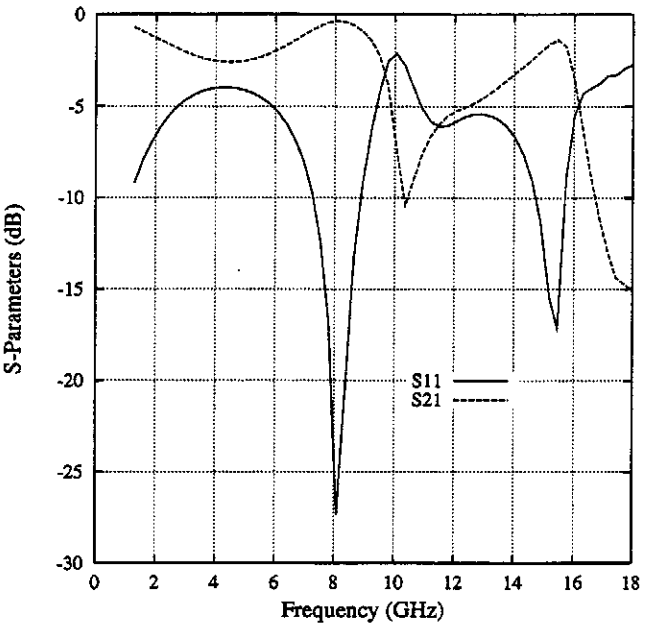

(b) Results with 3 truncated pairs of basic image sets.

Fig. 7. Scattering parameters of the structure in Fig. 2 when 2 and 3 specially truncated pairs of basic image sets are included in the analysis.

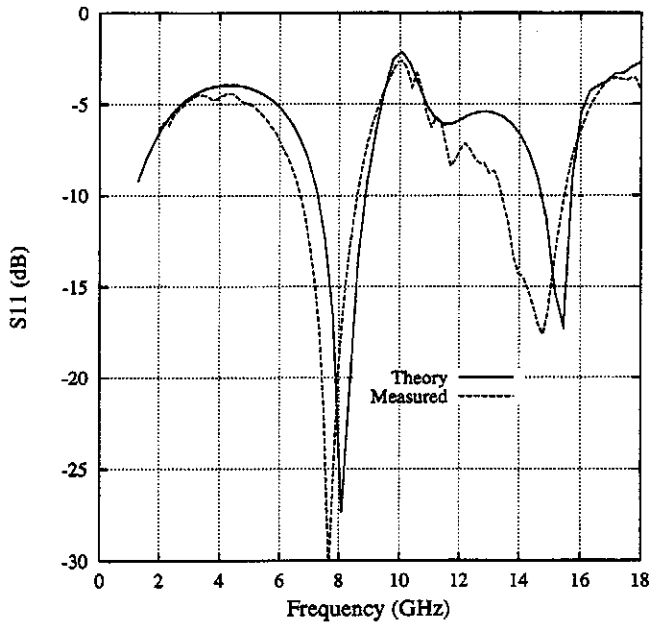

(a) S_{11} parameter.

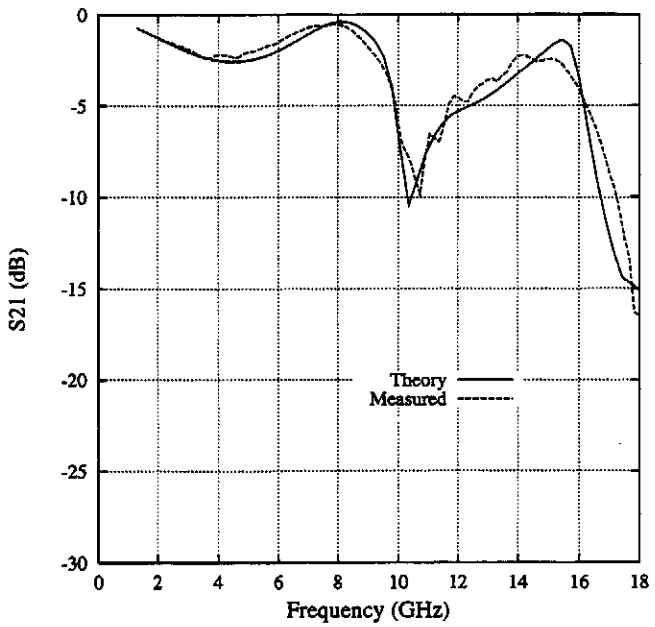

(b) S_{21} parameter.

Fig. 8. Measured versus simulated results for the scattering parameters of the structure in Fig. 2. Only 3 truncated pairs of basic image sets (14 images) are used in the theoretical prediction.

Fig. 9 we show the basic geometry of the antenna and the triangular meshes used in conjunction with the developed algorithms. For the analysis of this structure, adequate magnetic currents are defined at the cavity's top aperture and a set of coupled integral equations is defined and solved in the fashion described in [10]. In these equations, all electromagnetic interactions are computed with the specially truncated set of images derived in this paper. Fig. 10 presents measured versus simulated results for the S-parameters of the antenna when the upper patch is removed, and Fig. 11 for the complete antenna structure, with the upper patch on top, showing in all cases good agreement. An interesting feature of the technique derived is the rate of convergence of the numerical results when the number of specially truncated images is increased. For this last example no significance numerical difference is observed with 10 and 14 images, thus indicating good and fast convergence of the developed series.

V. Conclusions

In the frame of IE-MoM, a new contribution to the analysis of arbitrary shielded microwave circuits and cavity backed antennas has been presented. Following the proposed approach, Green's functions are formulated with well known Sommerfeld integrals and the know-how already available in this field is reused. The presence of lateral metallic walls is taken into account by using standard image theory and the convergence conditions of the resulting image series have been investigated. When slow convergence occurs, a specially truncated set of images has been derived, based on the rigorous imposition of the boundary conditions for the fields and potentials at the metallic walls. Results reveal that convergence using the specially truncated set of images is very fast and that with only 10-14 images accurate results are obtained. Moreover, the use of the technique described simply adds few analytical operations to the basic Sommerfeld formalism so that efficient computer codes can still be developed. In this paper measured and simulated results are compared for a stacked patch antenna with both patches exhibiting a complicated shape.

References

[1] J. Ching Cheng, H. I. Dib, and L. P. B. Katehi, "Theoretical modeling of cavity-backed patch antennas using a hybrid technique," *IEEE Transactions on Antennas and Propagation*, vol. 43, pp. 1003–1013, September 1995.

[2] J. C. Rautio and R. F. Harrington, "An electromagnetic time-harmonic analysis of shielded microstrip circuits," *IEEE Transactions on Microwave Theory and Techniques*, vol. 35, pp. 726–730, November 1987.

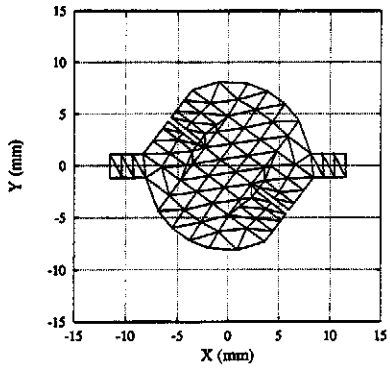

(a) Mesh lower patch.

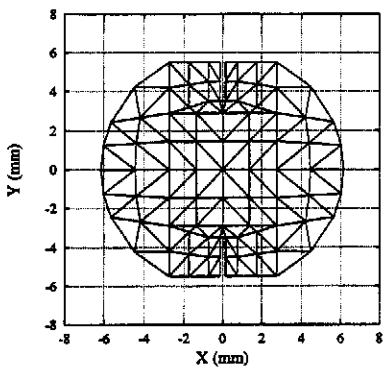

(b) Mesh upper patch.

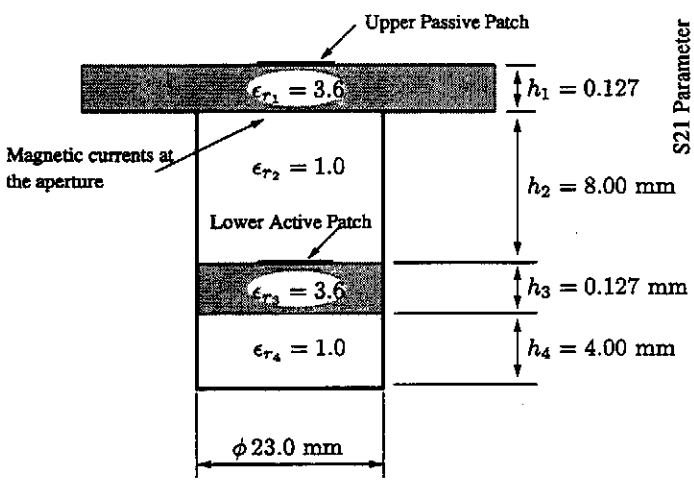

(c) Layered structure.

Fig. 9. Geometry of the double patch cavity-backed antenna analyzed in this paper.

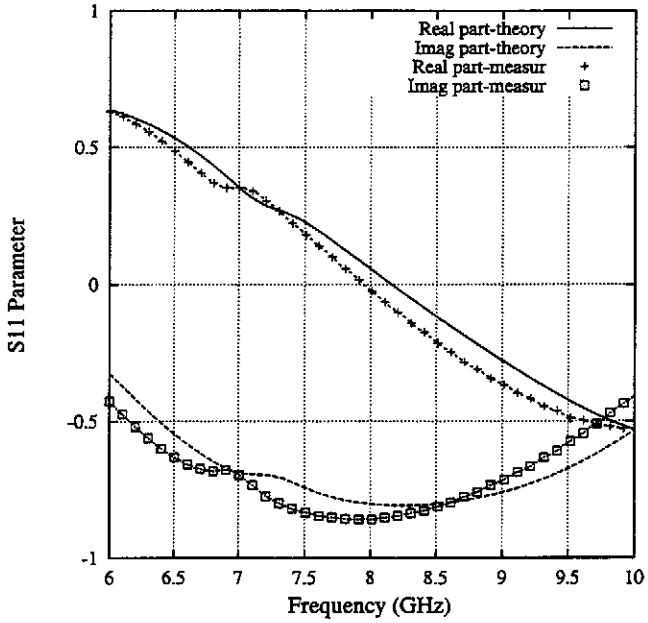

(a) S_{11} parameter.

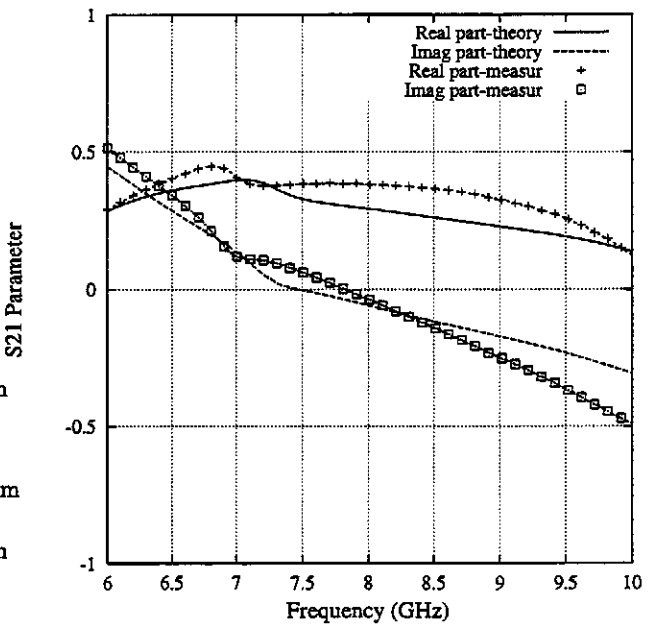

(b) S_{21} parameter.

Fig. 10. Measured versus simulated results for the antenna in Fig. 9 when the upper patch is removed. Real and imaginary part of the S-parameters are given.

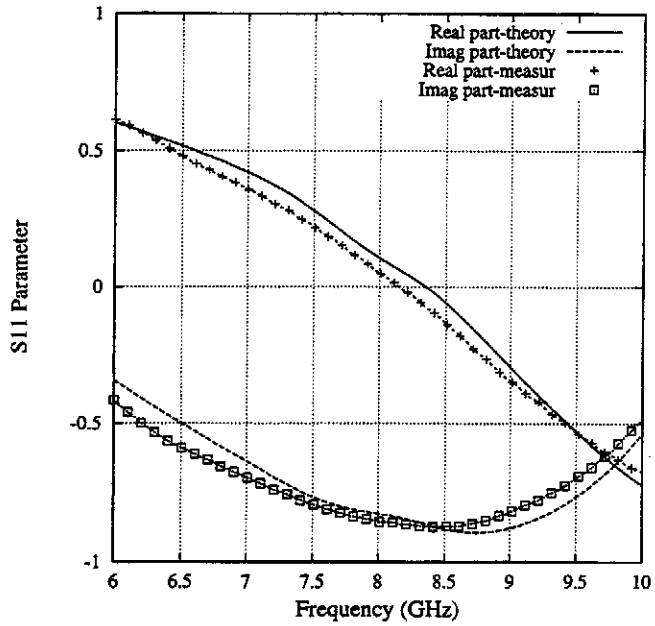

(a) S_{11} parameter.

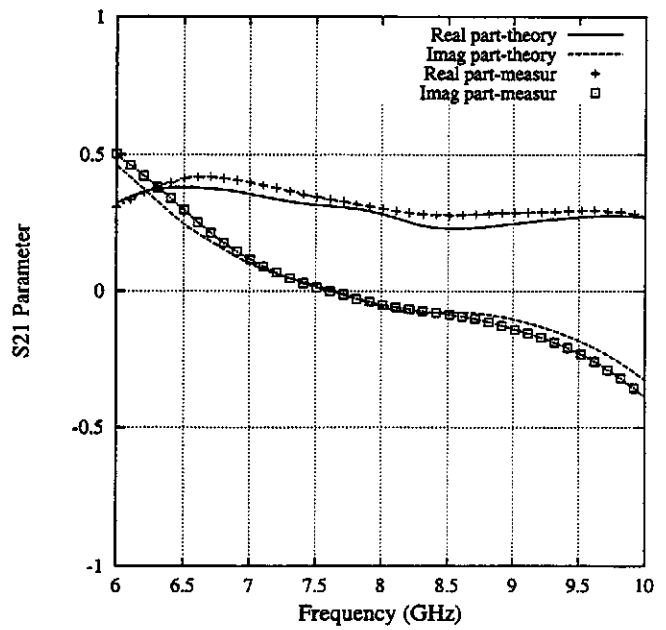

(b) S_{21} parameter.

Fig. 11. Measured versus simulated results for the antenna in Fig. 9 when the upper patch is placed on top. Real and imaginary part of the S-parameters are given.

[3] A. Hill and V. K. Tripathi, "An efficient algorithm for the three-dimensional analysis of passive microstrip components and discontinuities for microwave and millimeter-wave integrated circuits," *IEEE Transactions on Microwave Theory and Techniques*, vol. 39, pp. 83–91, January 1991.

[4] S. Hashemi-Yeganeh, "On the summation of double infinite series field computations inside rectangular cavities," *IEEE Transactions on Microwave Theory and Techniques*, vol. 43, pp. 641–646, March 1995.

[5] G. V. Eleftheriades, J. R. Mosig, and M. Guglielmi, "A fast integral equation technique for shielded planar circuits defined on nonuniform meshes," *IEEE Transactions on Microwave Theory and Techniques*, vol. 44, pp. 2293–2296, December 1996.

[6] M. Joo Park and S. Nam, "Efficient calculation of the green's function in rectangular waveguides," in *Proc. of the AP-S Symposium*, (Montreal, Canada), pp. 2354–2357, IEEE AP-S, 13-18 July 1997.

[7] G. G. Gentili, L. E. Garcia-Castillo, M. Salazar Palma, and F. Perez-Martinez, "Green's function analysis of single and stacked rectangular microstrip patch antennas enclosed in a cavity," *IEEE Transactions on Antennas and Propagation*, vol. 45, pp. 573–579, April 1997.

[8] K. A. Michalski and J. R. Mosig, "Multilayered media green's functions in integral equation formulations," *IEEE Transactions on Antennas and Propagation*, vol. 45, pp. 508–519, March 1997.

[9] J. R. Mosig and A. Alvarez Melcón, "Green's functions in layered media: imaginary axis integration and asymptotic behavior," in *Proc. of the AP-S Symposium*, (Baltimore, Maryland, USA), pp. 416–419, IEEE AP-S, 21-26 July 1996.

[10] J. R. Mosig, *Integral equation techniques for three-dimensional microstrip structures*, ch. 6: in The Review of Radio Science, pp. 127–152. Oxford University Press, 1990-1992. Ed. by Ross Stone.